Published in final edited form as:

Angew Chem Int Ed Engl. 2023 April 11; 62(16): e202300003. doi:10.1002/anie.202300003.

High-Porosity Metal–Organic Framework Glasses

Dr. Wentao Xu,
Department of Chemistry and Kavli Energy Nanoscience Institute, University of California, Berkeley, Berkeley, CA 94720, United States

Dr. Nikita Hanikel,
Department of Chemistry and Kavli Energy Nanoscience Institute, University of California, Berkeley, Berkeley, CA 94720, United States

Dr. Kirill A. Lomachenko,
European Synchrotron Radiation Facility, 71 Avenue des Martyrs, CS 40220, 38043 Grenoble Cedex 9, France

Dr. Cesare Atzori,
European Synchrotron Radiation Facility, 71 Avenue des Martyrs, CS 40220, 38043 Grenoble Cedex 9, France

Dr. Alicia Lund,
Department of Chemistry University of California, Berkeley, Berkeley, CA 94720, United States

Dr. Hao Lyu,
Department of Chemistry and Kavli Energy Nanoscience Institute, University of California, Berkeley, Berkeley, CA 94720, United States

Zihui Zhou,
Department of Chemistry and Kavli Energy Nanoscience Institute, University of California, Berkeley, Berkeley, CA 94720, United States

Dr. C. Austen Angell[†] **[Prof.]**,
School of Molecular Sciences, Arizona State University, Tempe, AZ 85287, United States

Dr. Omar M. Yaghi [Prof.]
Department of Chemistry, Kavli Energy Nanoscience Institute, and Bakar Institute of Digital Materials for the Planet, Division of Computing, Data Science, and Society, University of California, Berkeley Berkeley, CA 94720, United States

KACST−UC Berkeley Center of Excellence for Nanomaterials for Clean Energy Applications, King Abdulaziz City for Science and Technology Riyadh 11442, Saudi Arabia

Abstract

We report a synthetic strategy to link titanium-oxo (Ti-oxo) clusters into metal−organic framework (MOF) glasses with high porosity though the carboxylate linkage. A new series of MOF glasses were synthesized by evaporation of solution containing Ti-oxo clusters $Ti_{16}O_{16}(OEt)_{32}$,

[*] yaghi@berkeley.edu .
[†] Deceased 2021

linkers, and *m*-cresol. The formation of carboxylate linkages between the Ti-oxo clusters and the carboxylate linkers was confirmed by Fourier-transform infrared (FT-IR) spectroscopy. The structural integrity of the Ti-oxo clusters within the glasses was evidenced by both X-ray absorption near edge structure (XANES) and ^{17}O magic-angle spinning (MAS) NMR. After ligand exchange and activation, the fumarate-linked MOF glass, termed Ti-Fum, showed a N_2 Brunauer–Emmett–Teller (BET) surface areas of 923 m^2 g^{-1}, nearly three times as high as the phenolate-linked MOF glass with the highest BET surface area prior to this report.

Entry for the Table of Contents

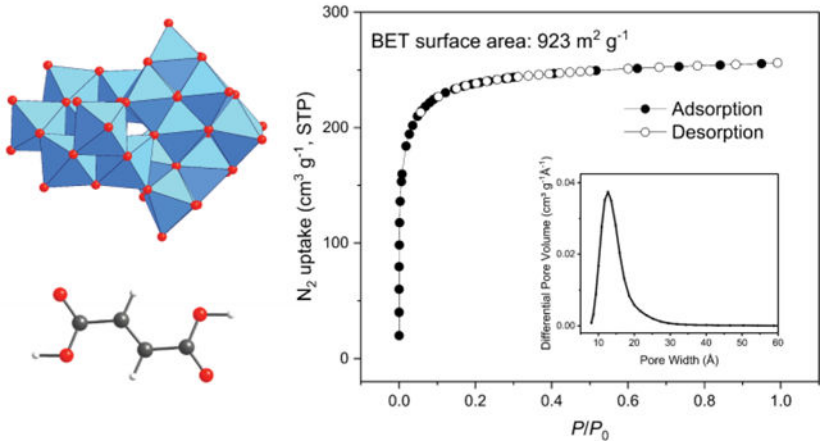

Metal−organic framework (MOF) glasses of carboxylate linkages were synthesized by reacting Ti-oxo clusters with carboxylic acid linkers. The activated MOF glass showed a N_2 Brunauer–Emmett–Teller (BET) surface areas of 923 m^2 g^{-1}, nearly three times as high as the phenolate-linked MOF glass with the highest BET surface area prior to this report.

Keywords

metal−organic framework (MOF) glasses; titanium-oxo (Ti-oxo) clusters; porosity; X-ray absorption near edge structure

---

Application of the principles of reticular chemistry[1,2] allows the construction of metal−organic framework (MOF) glasses through linking metal clusters (or ions) with organic molecules into transparent, amorphous, and monolithic solids.[3–5] By employing strong and directional coordination bonds between the building blocks, permanently porous MOF glasses with interconnected micropores that are accessible to guest molecules can be made as monoliths,[6] making them useful for gas storage and separations,[7–9] sensing,[10] energy storage,[11] and catalysis.[4] Although previous reports demonstrated MOF glasses with permanent porosity, their N_2 Brunauer–Emmett–Teller (BET) surface areas were only on the order of 100 m^2 g^{-1},[6] which is at least one order of magnitude lower than their crystalline counterparts.[12–14] A higher porosity would be required to harness the full potential of MOF glasses, this is impeded by their weak connectivity, thus making their pores architecturally frail.

Herein, we demonstrate a new synthetic strategy by utilizing the carboxylate linkage to reticulate titanium-oxo (Ti-oxo) clusters into MOF glasses leading to significantly improved BET surface areas of greater than 900 $m^2\ g^{-1}$. We employed the carboxylate binding group—yet unexplored in MOF glass chemistry, as it was anticipated to exhibit stronger binding affinity towards the Ti species than the previously utilized Bisphenol A and Bisphenol P linkers.[6,15] Its propensity to undergo bridging and chelating binding modes, was expected to give robust linkages and therefore permanently porous architectures. This allowed complete substitution of the deployed bulky modulating and structure-directing reagent (residing in the pores) without damaging the integrity of the structure; an aspect that was of significant concern and limiting in the previous report on the phenolate-based glasses.[6]

The first in a series of carboxylate-linked MOF glasses we report here is Ti-Fum. It was synthesized by slow evaporation of a solution containing the cluster $Ti_{16}O_{16}(OEt)_{32}$, fumaric acid, and *m*-cresol in an ethanol/tetrahydrofuran mixture until it turned into transparent glass [Figure 1a and Supporting Information (SI) Section S2]. Similar to phenolate-linked MOF glasses, the as-synthesized Ti-Fum exhibited a red color (Figure S1). This strong absorption in the visible-light range can be explained by ligand-to-metal charge transfer (LMCT) between the $O_{phenolate}$ and Ti^{IV} orbitals.[16] The existence of *m*-cresolate inside the as-synthesized Ti-Fum was also confirmed by ^{1}H-NMR spectroscopy of the fully hydrolyzed (digested) sample (SI Section S2 and S6). Formation of coordination bonds between the Ti-oxo cluster and the carboxylate linker was evidenced by Fourier-transform infrared (FT-IR) spectroscopy. Two new bands, not observed in the reactants, appeared at $\nu_{CO_2^-,symm}$ = 1390 cm^{-1} and $\nu_{CO_2^-,assymm}$ = 1514 cm^{-1} in the as-synthesized sample (Figure 1b). These two bands can be assigned to the symmetric and asymmetric stretches of the bridging, coordinated carboxylate groups, with a band splitting of $\Delta\nu$ = 124 cm^{-1} that is common in Ti-carboxylate compounds.[17–19] Broadening of the Ti–O stretching and Ti–O–Ti bending bands in the 400–750 cm^{-1} region further corroborates a reaction between the linker molecule and the Ti-oxo cluster (Figure S2).[19]

Post-synthetic modification of Ti-Fum was carried out by immersing the as-synthesized MOF glass in an excess amount of anhydrous methanol to allow the substitution reaction between *m*-cresol and methanol. The methanol-exchanged Ti-Fum was further activated under dynamic vacuum (~10^{-3} mbar) to remove the residual solvent inside the pores. The activated Ti-Fum monolith exhibited an orange color (Figure 1d). Successful removal of *m*-cresol and unbound methanol was confirmed by elemental analysis and ^{1}H-NMR spectroscopy of the digested sample, where a chemical formula of $Ti_{16}O_{16}(fumarate)_{6.8}(methoxide)_{18.4}$ was found for the activated MOF glass (SI Section S2). Specifically, the ratio of fumarate to methoxide was obtained from ^{1}H-NMR results (1:2.69) and, through charge balancing consideration, the corresponding exact number was achieved and further confirmed by elemental analysis. Along with *m*-cresolate, unbound linkers were also removed during the methanol treatment, which was tracked by the disappearance of the absorption bands at $\nu_{C=O}$ = 1668 and ν_{C-O} =1263 cm^{-1} in the FT-IR spectrum, belonging to the asymmetric C=O and C–O stretches of fumaric acid, respectively (Figure 1b and Figure S3).[20] No significant changes were observed in the symmetric and asymmetric vibration

modes of the coordinated carboxylate groups in the FT-IR spectrum, indicating that the bridging carboxylate linkage is preserved during the removal of *m*-cresolate from the MOF glass.[21]

Powder X-ray diffraction (PXRD) analysis of the activated Ti-Fum was conducted using Cu Kα radiation. Ti-Fum exhibited one very broad peak at $2\theta = 10.4°$, corresponding to a *d*-spacing of 8.5 Å, thus indicating the presence of some degree of local order in the otherwise amorphous MOF glass (Figure 1c). The coherently scattering domain size was calculated to be 2.4 nm using the Scherrer equation,[22] which is 2–3 times of the estimated *d*-spacing. The presence of local order has also been observed in other materials prepared from Ti-oxo clusters. MOF glass with phenolate linkages Ti-BPA (BPA = 2,2-bis(4-hydroxyphenyl)propane) showed a *d*-spacing of 17.6 Å,[6] while a hybrid material termed TG-G1 exhibited a *d*-spacing between 19 and 21 Å with a domain size of 5–6 nm.[19]

The structural integrity of discrete Ti-oxo clusters inside the MOF glass after synthesis and post-synthetic modification was evidenced by X-ray absorption near edge structure (XANES). The position of the Ti K absorption edge and the low intensity of the pre-edge peaks (features A in Figure 2a) indicate the presence of predominantly 6-coordinated Ti^{4+} centers in significantly distorted octahedral environment.[23–25] The spectrum of Ti-Fum exhibits marked differences compared to those of metallic Ti, bulk Ti oxides (rutile and anatase), and small Ti-oxo clusters [$Ti_6O_6(OiPr)_6(AB)_6$, AB = 4-aminobenzoate] and $Ti_8O_8[OOC(CH_3)_3]_{16}$, which rules out the existence of significant amounts of such phases in the Ti-Fum MOF glass. Conversely, XANES of the discrete Ti_{16}-oxo cluster shows motives similar to those of Ti-Fum in all regions of the spectrum, supporting the presence of such units in the structure of the MOF glass. The broadening of the white-line features (peaks B and C) in the spectrum of Ti-Fum compared to those of the $Ti_{16}O_{16}(OEt)_{32}$ reference can be explained by a higher degree of local disorder in the Ti-oxo clusters incorporated into the glass.[23] Notably, these features become slightly sharper upon activation of the MOF glass, indicating a minor ordering effect rather than degradation, which confirms the overall stability of the Ti-Fum structure. Additionally, Ti K-edge EXAFS spectra of the materials indicate similarity between the structures of Ti-Fum (before and after activation) and the $Ti_{16}O_{16}(OEt)_{32}$ cluster, as well as structural discrepancy between the MOF glass and the $Ti_6O_6(O^iPr)_6(AB)_6$ and $Ti_8O_8[OOC(CH_3)_3]_{16}$ clusters (Figure S5), thus further supporting the XANES results.

The integrity of the Ti-oxo clusters within the MOF glass was further corroborated by ^{17}O magic-angle spinning (MAS) NMR. ^{17}O NMR is a powerful and widely used tool for differentiation of Ti-oxo clusters in both liquids and solids.[26] Typically, oxygen species of different coordination number and geometry show different chemical shifts and quadrupolar coupling parameters, thus resulting in unique resonances in the ^{17}O NMR spectrum for each Ti-oxo cluster. By comparing the ^{17}O NMR spectrum before and after the reaction, the integrity of the Ti-oxo clusters can be evaluated. ^{17}O-enriched water was used to selectively label the oxo bridges of the $Ti_{16}O_{16}$ core.[27]

The solid-state NMR spectrum of the ^{17}O-labeled $Ti_{16}O_{16}(OEt)_{32}$ cluster showed three sets of peaks located at 751, 550–590, and 380–400 ppm, corresponding to μ_2-O, μ_3-O,

and μ_4-O species, respectively (Figure 2b and c, and Table S1). These three sets of peaks were also observed in the ^{17}O NMR spectrum of Ti-Fum, implying the preservation of the $Ti_{16}O_{16}$ core during the MOF glass formation. We note that the peaks corresponding to the μ_4-O species exhibited a slight upfield shift but remained in the typical range of μ_4-O in Ti-oxo species.[26] The signals of all oxygen site types became broader upon glass formation, thus suggesting that the bridging oxygens are under a variety of slightly different chemical environments in the amorphous glass. Previously, broadening of NMR signals and appearance of asymmetric peak shapes as a result of increasing diversity in chemical environments has also been observed in TiO_2 sol-gels made from $Ti_{16}O_{16}(OEt)_{32}$.[27]

The ^{17}O NMR spectra of $Ti_{16}O_{16}(OEt)_{32}$ and activated Ti-Fum were fit using the program Dmfit[28] to evaluate the quadrupolar coupling of the ^{17}O species, which relates to the bonding, crystallographic symmetry, and molecular structure of the different ^{17}O species in the $Ti_{16}O_{16}$ cluster (Table S1).[27,29] No significant change of the quadrupolar coupling was observed within the error of the ^{17}O spectrum fit upon MOF glass formation, further suggesting that the clusters are still intact while connected into the framework by the linkers.

The porosity of Ti-Fum was examined by using nitrogen sorption analysis at 77 K (Figure 3). The carboxylate-linked MOF glass showed a Type I isotherm with a BET surface area of 923 $m^2\ g^{-1}$, nearly three times as high as Ti-BPA—the phenolate-linked MOF glass with the highest BET surface area prior to this report. Unlike crystalline MOFs, which usually exhibit a uniform pore structure, Ti-Fum showed a wide pore size distribution from 8 to around 20 Å in diameter, with the maximum at 13 Å. We attribute the record-breaking porosity of Ti-Fum to two factors: (i) complete removal of the bulky modulating and structure-directing *m*-cresolate molecules from the pores, and (ii) high connectivity between the Ti-based secondary building units (SBUs) indicated by the high linker-to-Ti ratio.

Removal of *m*-cresolate is the key step for creating micropores. When it was replaced by methoxide, porosity was generated inside the MOF glass. We estimated that a free space volume of 93 $Å^3$ is created for each *m*-cresolate molecule that gets replaced, and a total pore volume of 0.43 $cm^3\ g^{-1}$ can be achieved upon its complete substitution (SI Section S8). This estimation matches well with the experimental pore volume calculated from the nitrogen isotherm at P/P_0=0.99 (0.40 cm^3/g). For comparison, Ti-Fum treated with aprotic solvents (DMSO followed by acetone) showed negligible porosity (Figure S12). The importance of *m*-cresol as structure-directing reagent was additionally demonstrated by the fact that the sample synthesized in absence of *m*-cresol showed a BET surface area below 20 $m^2\ g^{-1}$ (Figure S14). While the robustness of the carboxylate linkage allowed the complete removal of *m*-cresolate without compromising the framework integrity. In contrast, significant amounts of residual *m*-cresolate were found in the phenolate-linked MOF glass.[6] We note that the residual *m*-cresolate not only occupied the pores but also increased the overall density of the framework, thus limiting the specific surface area of the glass. In addition to the complete substitution of *m*-cresolate, a relatively high connectivity between the Ti-oxo clusters in Ti-fum was inferred from elemental analysis. The respective results suggested a linker-to-Ti ratio of 0.43:1 (SI Sections S2 and S6), corresponding to 50–100% higher than the respective ratio in the previously reported phenolate-based MOF glasses deploying the same Ti-oxo clusters.[6] This relatively high linker-to-SBU ratio of Ti-Fum is

likely another important factor leading to its high porosity, as high SBU connectivity can be helpful in stabilizing the micropores and thus preventing structural collapse upon removal of guest molecules. This observation has been made in some crystalline MOFs, where higher connectivity between SBUs led to mechanically more robust frameworks.[30,31] The carboxylate linkage also contributes to the thermal stability of Ti-Fum as evidenced by results of thermogravimetric analysis of the glass under nitrogen atmosphere. Comparable to typical crystalline MOFs,[32–34] the carboxylate-based MOF glass exhibited the first decomposition step at a temperature higher than 300 °C (Figure S20). The residual weight of the MOF glass after thermogravimetric analysis in air was 49.9%, corresponding to 29.9% Ti in the form of TiO2 (Figure S21, S22). This number is in good agreement with the ICP-OES analysis, where 30.7% Ti was found in the activated Ti-Fum.

To demonstrate the modularity and versatility of our approach, two additional carboxylic acid linkers, furan-2,5-dicarboxylic acid (FDC) and thiophene-2,5-dicarboxylic acid (TDC), were used to synthesize transparent MOF glasses by employing the same design principles. This led to new glasses termed Ti-FDC and Ti-TDC, respectively, with surface areas significantly higher (400–500 m^2/g) than previously reported for phenolate-linked MOF glasses (Figure S15). The optimization of the porosity is ongoing. Ti K-edge XANES and EXAFS spectra of these two glasses were very similar to Ti-Fum, thus corroborating the identical local environment of the Ti^{4+} centers in the Ti-oxo clusters of all three glasses reported herein (Figure S4). The presence of sulfur in Ti-TDC also gave us the opportunity to study the linker distribution inside the MOF glass. A homogeneous distribution of linkers inside the Ti-TDC was confirmed by scanning electron microscopy with energy dispersive X-ray spectroscopy mapping (Figure S23). Overall, our results demonstrated a modular approach of using carboxylate linkages to access highly porous MOF glasses with permanent porosity decorated by a diverse pore environment.

Supplementary Material

Refer to Web version on PubMed Central for supplementary material.

Acknowledgements

We appreciate the support of KACST-UC Berkeley Center of Excellence for Nanomaterials for Clean Energy Applications. The European Synchrotron Radiation Facility (Grenoble, France) is acknowledged for granting beamtime for XANES measurements at the BM23 beamline. This study relied on the use of instruments located in the College of Chemistry Nuclear Magnetic Resonance (NMR) Facility, which are partially supported by NIH S10OD024998. We thank Prof. Yingbo Zhao for valuable discussions. N.H. is grateful for the support through a Kavli ENSI Philomathia Graduate Student Fellowship and a Blavatnik Innovation Fellowship.

References

[1]. Yaghi OM, Ockwig OKM,NW, Chae HK, Eddaoudi M, Kim J, Nature 2003, 423, 705–714. [PubMed: 12802325]

[2]. Yaghi OM, Kalmutzki MJ, Diercks CS, Introduction to Reticular Chemistry: Metal-Organic Frameworks and Covalent Organic Frameworks, Wiley-VCH, Weinheim, 2019.

[3]. Bennett TD, Horike S, Nat Rev Mater 2018, 3, 431–440.

[4]. Fonseca J, Gong T, Jiao L, Jiang HL, J Mater Chem A Mater 2021, 9, 10562–10611.

[5]. Ma N, Horike S, 2022, DOI 10.1021/acs.chemrev.1c00826.

[6]. Zhao Y, Lee SY, Becknell N, Yaghi OM, Angell CA, Yang P, Yaghi OM, Angell A, Division MS, Berkeley L, States U, J Am Chem Soc 2016, 138, 10818–10821.

[7]. Frentzel-Beyme L, Kloß M, Kolodzeiski P, Pallach R, Henke S, J Am Chem Soc 2019, 141, 12362–12371. [PubMed: 31288513]

[8]. Wang Y, Jin H, Ma Q, Mo K, Mao H, Feldhoff A, Cao X, Li Y, Pan F, Jiang Z, Angewandte Chemie - International Edition 2020, 59, 4365–4369. [PubMed: 31893511]

[9]. Lin R, Hou J, Li M, Wang Z, Ge L, Li S, Smart S, Zhu Z, Bennett TD, Chen V, Chemical Communications 2020, 56, 3609–3612. [PubMed: 32167111]

[10]. Thornton AW, Jelfs KE, Konstas K, Doherty CM, Hill AJ, Cheetham AK, Bennett TD, Chemical Communications 2016, 52, 3750–3753. [PubMed: 26800518]

[11]. Jiang G, Qu C, Xu F, Zhang E, Lu Q, Cai X, Hausdorf S, Wang H, Kaskel S, Adv Funct Mater 2021, 31, DOI 10.1002/adfm.202104300.

[12]. Furukawa H, Ko N, Go YB, Aratani N, Choi SB, Choi E, Yazaydin a O., Snurr RQ, O'Keeffe M, Kim J, Yaghi OM, Science (1979) 2010, 329, 424–428.

[13]. Farha OK, Eryazici I, Jeong NC, Hauser BG, Wilmer CE, Sarjeant AA, Snurr RQ, Nguyen ST, Yazaydin AÖ, Hupp JT, J Am Chem Soc 2012, 134, 15016–15021. [PubMed: 22906112]

[14]. Hönicke IM, Senkovska I, Bon V, Baburin IA, Bönisch N, Raschke S, Evans JD, Kaskel S, Angewandte Chemie - International Edition 2018, 57, 13780–13783. [PubMed: 30160076]

[15]. Boyle TJ, Tyner RP, Alam TM, Scott BL, Ziller JW, Potter BG, J Am Chem Soc 1999, 121, 12104–12112.

[16]. Assi H, Mouchaham G, Steunou N, Devic T, Serre C, Chem Soc Rev 2017, 46, 3431–3452. [PubMed: 28537319]

[17]. Thiele K-H, Panse M, Z Anorg Allg Chem 1978, 441, 23–28.

[18]. Doeuff S, Dromzee Y, Taulelle F, Sanchez C, Inorg Chem 1989, 28, 4439–4445.

[19]. Soler-Illia GJDAA, Rozes L, Boggiano MK, Sanchez C, Turrin CO, Caminade AM, Majoral JP, Angewandte Chemie - International Edition 2000, 39, 4250–4254.

[20]. Nájera JJ, Percival CJ, Horn AB, Physical Chemistry Chemical Physics 2009, 11, 9093–9103. [PubMed: 19812829]

[21]. Dan-Hardi M, Serre C, Frot T, Rozes L, Maurin G, Sanchez C, Férey G, J Am Chem Soc 2009, 131, 10857–10859. [PubMed: 19621926]

[22]. Patterson AL, Physical Review 1939, 56, 978–982.

[23]. Farges F, Brown GE, Phys Rev B Condens Matter Mater Phys 1997, 56, 1809–1819.

[24]. Fernández-García M, Belver C, Hanson JC, Wang X, Rodriguez JA, J Am Chem Soc 2007, 129, 13604–13612. [PubMed: 17927180]

[25]. Berardi S, Kopula Kesavan J, Amidani L, Meloni EM, Marelli M, Boscherini F, Caramori S, Pasquini L, ACS Appl Mater Interfaces 2020, 12, 47435–47446. [PubMed: 32986954]

[26]. Rozes L, Sanchez C, Chem Soc Rev 2011, 40, 1006–1030. [PubMed: 21218224]

[27]. Scolan E, Magnenet C, Massiot D, Sanchez C, J Mater Chem 1999, 9, 2467–2474.

[28]. Massiot D, Fayon F, Capron M, King I, le Calvé S, Alonso B, Durand JO, Bujoli B, Gan Z, Hoatson G, Magnetic Resonance in Chemistry 2002, 40, 70–76.

[29]. Ashbrook SE, Farnan I, Solid State Nucl Magn Reson 2004, 26, 105–112. [PubMed: 15276641]

[30]. Dissegna S, Vervoorts P, Hobday CL, Düren T, Daisenberger D, Smith AJ, Fischer RA, Kieslich G, J Am Chem Soc 2018, 140, 11581–11584. [PubMed: 30169021]

[31]. Kapustin EA, Lee S, Alshammari AS, Yaghi OM, ACS Cent Sci 2017, 3, 662–667. [PubMed: 28691079]

[32]. Chui SSY, Lo SMF, Charmant JPH, Orpen AG, Williams ID, Science 1999, 283, 1148–1150. [PubMed: 10024237]

[33]. Li H, Eddaoudi M, O'Keeffe M, Yaghi OM, Nature 1999, 402, 276–279.

[34]. Healy C, Patil KM, Wilson BH, Hermanspahn L, Harvey-Reid NC, Howard BI, Kleinjan C, Kolien J, Payet F, Telfer SG, Kruger PE, Bennett Coord TD. Chem. Rev 419, 213388.

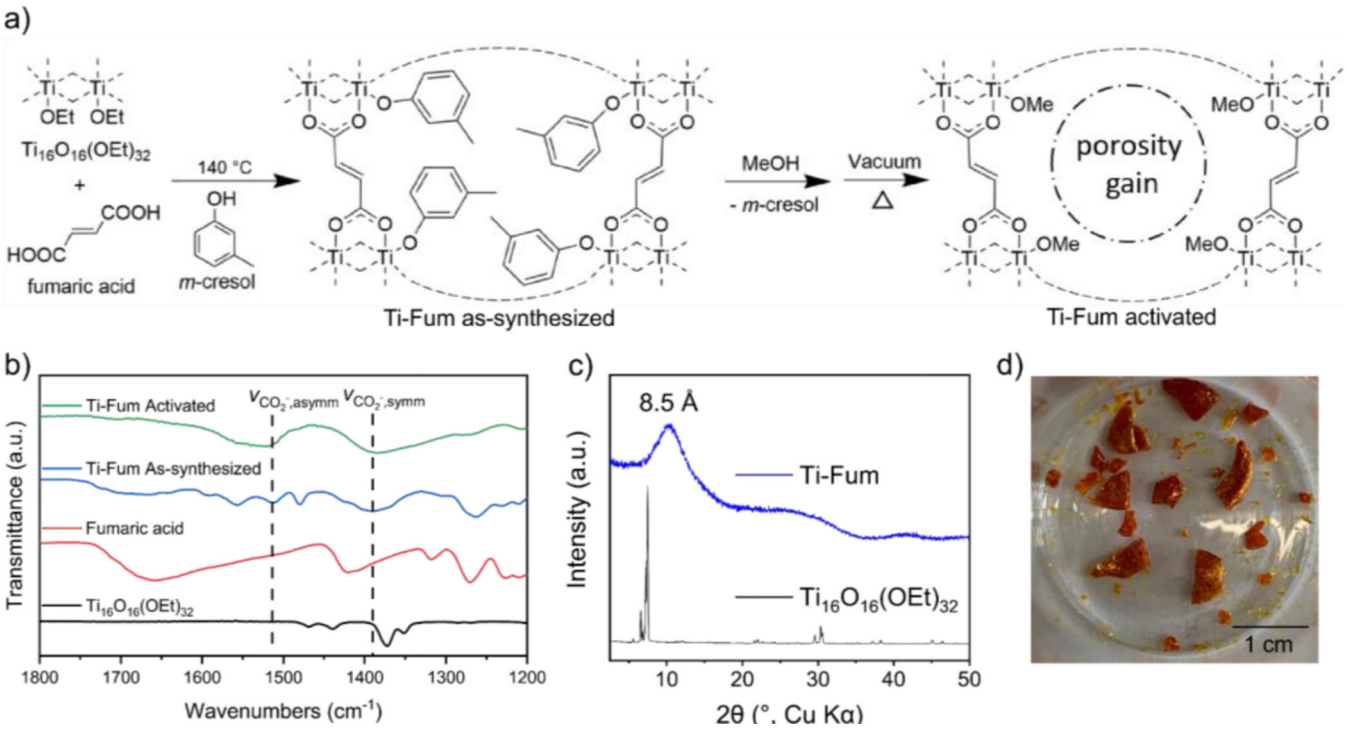

Figure 1.

(a) Proposed mechanism of synthesis and activation of Ti-Fum. Some structural elements, such as the bridging oxygens, are omitted and indicated by dashed lines for clarity. (b) FT-IR spectra of as-synthesized and activated Ti-Fum, fumaric acid, as well as $Ti_{16}O_{16}(OEt)_{32}$. (c) PXRD patterns of Ti-Fum and $Ti_{16}O_{16}(OEt)_{32}$. Broad peak at $2\theta = 10.4°$ correspond to a *d*-spacing of 8.5 Å.(d) Photograph of activated Ti-Fum.

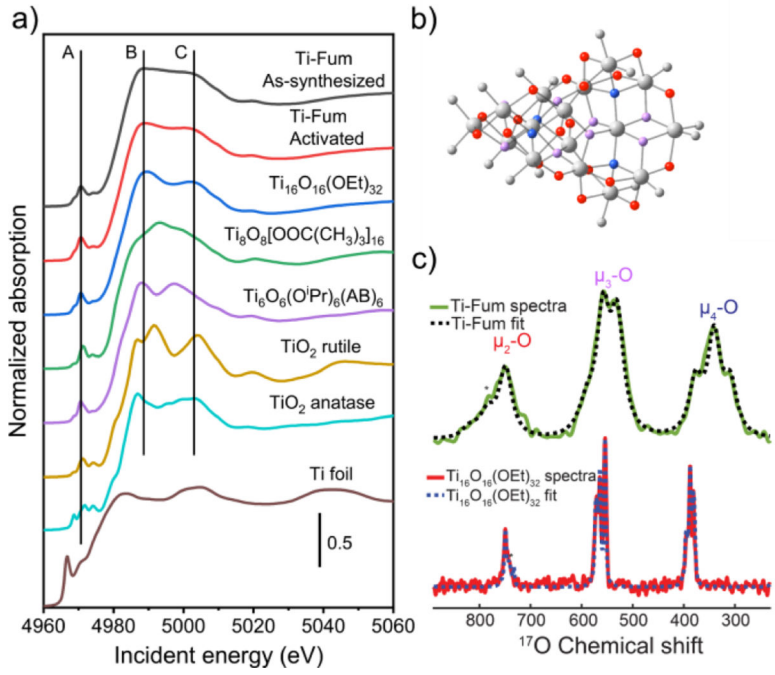

Figure 2.

Structural integrity of Ti-oxo clusters in Ti-Fum. (a) Ti K-edge XANES spectra of as-synthesized and activated Ti-Fum, isolated Ti-oxo clusters of various sizes, Ti oxides, and metallic Ti. The spectra are shifted along the vertical axis for the sake of clarity. (b) Structure of the $Ti_{16}O_{16}(OEt)_{32}$ core with μ_2-O, μ_3-O, and μ_4-O labeled in red, lavender, and blue, respectively. Ti and ethoxy-O are displayed in gray; ethyl groups are omitted for clarity. (c) ^{17}O MAS NMR of ^{17}O-labeled activated Ti-Fum and $Ti_{16}O_{16}(OEt)_{32}$

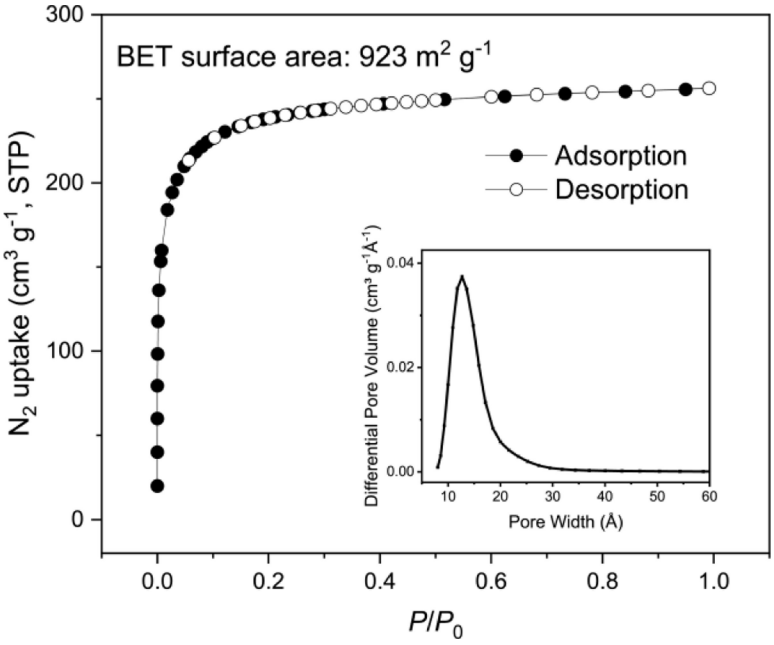

Figure 3.
N_2 sorption isotherm and pore-size distribution (inset) of Ti-Fum at 77K.